Electronic Supplementary Material (ESI) for Physical Chemistry Chemical Physics.

Radiation effects, zero thermal expansion, and pressure-induced phase transition in $CsMnCo(CN)_6$

SUPPORTING INFORMATION

Hanna L. B. Boström,[a*] Andrew B. Cairns,[b,c] Muzi Chen,[b,c]
Dominik Daisenberger,[d] Christopher J. Ridley,[e] and Nicholas P. Funnell[e]

[a] Max Planck Institute for Solid State Research, Heisenbergstraße 1,
D-70569 Stuttgart, Germany.
[b] Department of Materials, Imperial College London, Royal School of Mines,
Exhibition Road, SW7 2AZ, London, U.K.
[c] London Centre for Nanotechnology, Imperial College London, SW7 2AZ, London, U.K.
[d] Diamond Light Source Ltd., Harwell Campus, Didcot OX11 0DE, U.K.
[e] ISIS Neutron and Muon Source, Rutherford Appleton Laboratory,
Harwell Campus, Didcot OX11 0QX, U.K.

*To whom correspondence should be addressed;
E-mail: h.bostroem@fkf.mpg.de

Contents

1 Experimental details

Polycrystalline samples of $CsMnCo(CN)_6$ were synthesised by direct combination of reagents. In a typical synthesis, a solution of $MnSO_4{\cdot}H_2O$ or $MnCl_2$ (0.35 mmol) in 0.5 ml H_2O was added dropwise to a solution of $K_3Co(CN)_6$ (0.35 mmol) in 0.5 ml H_2O, saturated with ∼30-fold excess of CsCl. The reaction mixture was stirred at 50 °C for 2 h and the resulting white powder collected by filtration or centrifugation. Different sample batches were used for the experiment at I11, I15, and PEARL, respectively. The composition of the sample studied at I11 was confirmed by inductively coupled plasma (ICP) by a Perkin Elmer ICP-OES Avio 200 spectrometer. The samples were heated to 600 °C for 6 h prior to dissolution in aqua regia and dilution using ICP grade water. The plasma was ignited using Ar gas and the instrument allowed to thermally stabilise for 5 min. For the remaining samples, elemental analysis was carried out by a Varian Vista-PRO ICP-OES spectrometer with axial plasma (Fa. Variant Darmstadt). The sample was dissolved in 65% HNO_3 at 185 °C for 25 min *via* microwave digestion using a Discover SP-D from CEM GmbH and then diluted with doubly distilled water. In all cases, ICP values were close to 1:1 ratio of Mn:Co, which justifies our comparison of different sample batches, and hence, the ideal stoichiometry of $CsMnCo(CN)_6$ was used in the refinements.

Variable-temperature diffraction data were collected at the high-resolution powder diffraction beamline, I11, at Diamond Light Source, U.K. Individual data sets were collected using a Mythen2 Position Sensitive Detector (PSD) with two 2-second scans separated by an angular shift in detector position of 2.5°. The wavelength, zero-point error, and intrinsic peak-shape parameters were refined against a known Si 640c NIST standard. To investigate the possibility of beam-induced strain effects, 10 measurements were carried on the same part of the sample with 5 s wait time between successive scans. The variable-temperature diffraction patterns were measured on cooling from 500 to 85 K using an Oxford cryostream. To avoid lattice parameter changes due to radiation effects, the capillary was translated between every measurement during the variable-temperature data collection. The capillary was changed between 300 K and 260 K, but both capillaries were prepared from the same sample batch.

Variable-pressure powder X-ray diffraction was performed on beamline I15 at Diamond Light Source, at an energy of 33 keV. $CsMnCo(CN)_6$ was dried at 80 °C under a vacuum for >24 h prior to being loaded into a diamond anvil cell (DAC), with Daphne 7373 oil as a pressure-transmitting medium and a ruby for pressure calibration. To minimise radiation damage, the beam intensity was attenuated with aluminium plates. The sample-to-detector distance was calibrated following standard procedures from the diffraction ring of a LaB_6 standard. The best-scattering sample

position of the cell (position 1) was measured at every pressure point, and to check for beam damage, data from other sample positions were periodically sampled. As no strong effects of the radiation on the lattice parameters or data quality were found, only data from position 1 are presented here. The data were processed using Dioptas.[S1]

Variable-pressure neutron powder diffraction was carried out on the PEARL diffractometer[S2] at the ISIS Neutron and Muon source, U.K. The ground powder was heated to 100 °C under vacuum before loading in a null-scattering TiZr gasket along with a Pb pressure marker, and placed between single-toroid ZrO_2-toughened Al_2O_3 anvils. The pressure-transmitting medium was a perdeuterated methanol–ethanol mixture in a 4:1 volume ratio. The anvil assembly was then loaded in a V3 Paris-Edinburgh press and mounted in the PEARL instrument. Pressure was controlled *via* an oil-driven piston. The data were processed using Mantid.[S3]

Analysis of powder diffraction patterns was carried out by Pawley and Rietveld refinements using the software TOPAS.[S4–6] Rietveld refinement of $CsMnCo(CN)_6$ was carried out at ambient conditions against X-ray data and at 3.7 GPa against both X-ray and neutron data, and the lattice parameters as a function of X-ray exposure, temperature, and pressure were extracted by Pawley refinements. For the I11 data, the peak shape was found from a standard, and a Lorentzian strain term was applied to account for sample-dependent broadening. For the neutron data, the peak shape was modelled as a pesudo-Voigt function convoluted with a back-to-back double exponential, and for the I15 data, the modified Thompson-Cox-Hastings pseudo-Voigt was used. In the X-ray data, an additional Lorentzian *hkl*-dependent peak broadening was added to account for the anisotropic peak shapes caused by Cs disorder.

For the Rietveld refinements, the Cs occupancies of the two crystallographically inequivalent sites in $F\bar{4}3m$ were refined subject to the constraint that total occupancy agreed with the elemental analysis. The high-pressure phase was refined against both X-ray and neutron data, using symmetry modes as implemented in the software ISODISTORT.[S7] The patterns were weighted to give equal contributions to R_{wp}, to prevent the refinement to be dominated by the more intense XRD pattern. The symmetric strain (Γ_1^+) and octahedral tilt (X_3^+) were refined. Additional order parameters (Γ_3^+ and X_4^-) corresponding to tetragonal strain and distortions of the octahedra are also present, but refinement of these parameters did not significantly improve the fit; hence their amplitudes were fixed at zero.

The lattice parameters as a function of X-ray exposure, temperature, and pressure were extracted using Pawley refinements. The coefficient of thermal expansion was calculated using PASCal.[S8] The variable-pressure unit cell lattice parameters were fitted using the third-order Murnaghan equation of state as implemented in the software EoSfit-GUI.[S9, S10]

2 Variable-radiation dose data

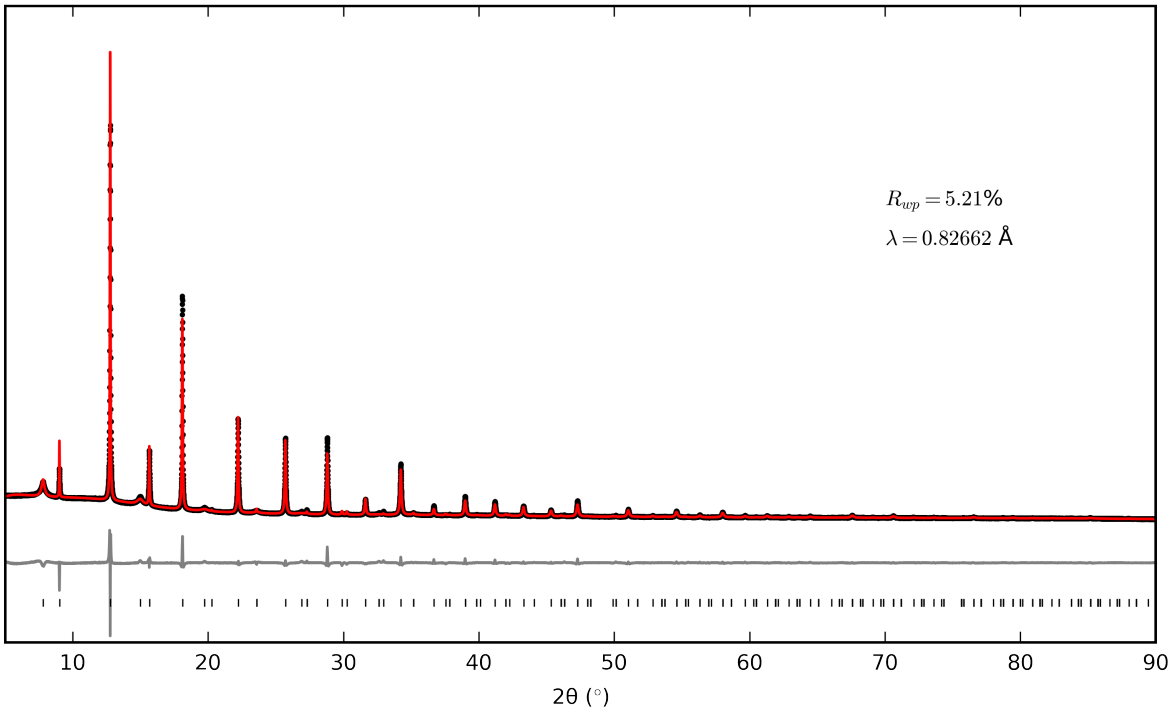

Figure S1: The Rietveld fit of the ambient phase of $CsMnCo(CN)_6$ in $F\bar{4}3m$. Experimental data are shown in black, the fit in red, the residuals in grey and allowed reflections indicated by vertical bars.

Table S1: Crystallographic details determined by Rietveld refinement of PXRD data for $CsMnCo(CN)_6$ at ambient conditions. Data collected at I11, Diamond Light Source.

Space group	$F\bar{4}3m$
a / Å	10.50713(3)
V / Å^3	1159.986(11)
Z	4
R_{wp}	5.21%

Atom	occ	Wyckoff site	x	y	z	B_{iso}* / Å^2
Cs	0.7637(16)	4c	0.25	0.25	0.25	1.89(3)
Cs	0.2363(16)	4d	0.75	0.25	0.25	1.89
Mn	1	4a	0	0	0	1.71(3)
Co	1	4b	0	0	0.5	1.71
C	1	24f	0	0	0.300(3)	1.71
N	1	24f	0	0	0.204(2)	1.71

* B_{iso} constrained to be equal for the Cs atoms and for the framework atoms.

Table S2: Lattice parameters of $CsMnCo(CN)_6$ as a function of increased X-ray dose.

measurement number	a / Å
1	10.51072(3)
2	10.51064(3)
3	10.51054(3)
4	10.51049(3)
5	10.51042(3)
6	10.51039(3)
7	10.51037(3)
8	10.51035(3)
9	10.51030(3)
10	10.51027(3)

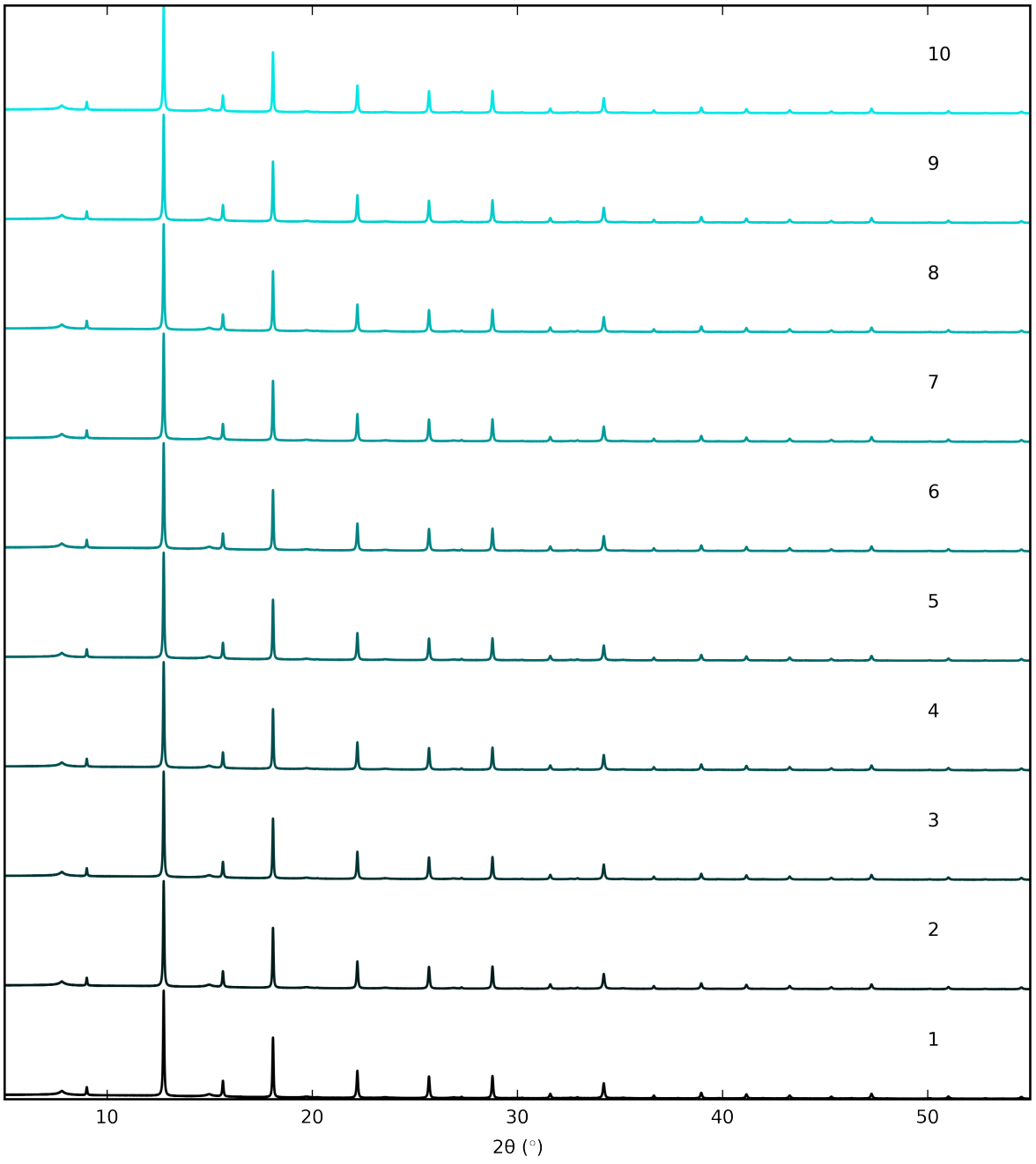

Figure S2: X-ray diffraction patterns of $CsMnCo(CN)_6$ from the same part of the sample such that the X-ray dose increases linearly with measurement number. The intensities of the most intense reflection are normalised to unity. $\lambda = 0.82662\,\text{Å}$.

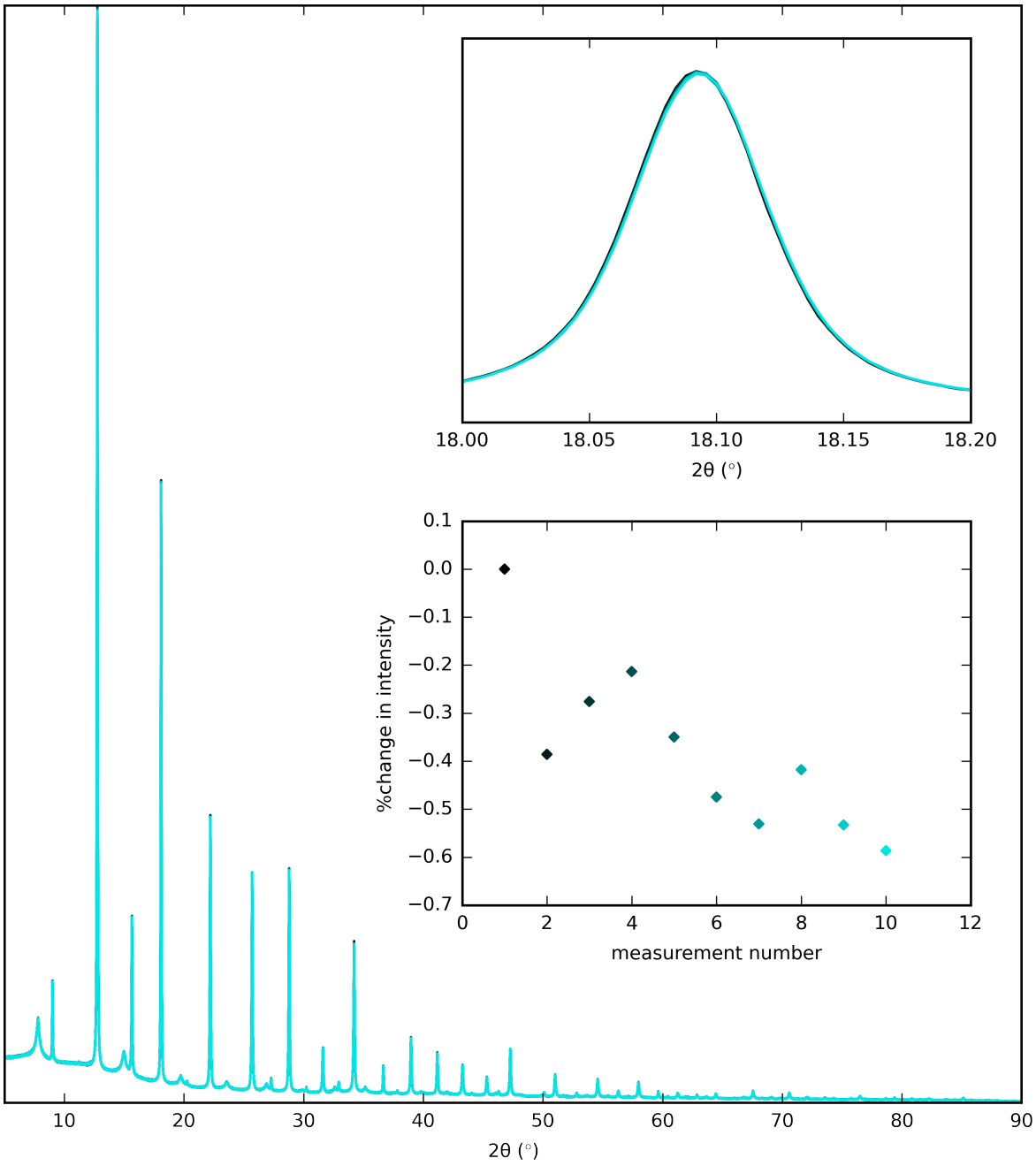

Figure S3: Overlay of X-ray diffraction patterns of $CsMnCo(CN)_6$ as a function of increased X-ray dose, indicated by increasing cyan colour. The insets show an enlarged view of the 400 reflection and the change in intensity of the most intense reflection (220) as a function of radiation exposure. $\lambda = 0.82662\,\text{Å}$.

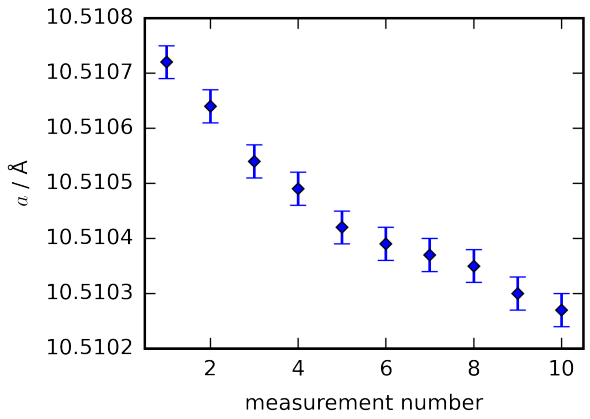

Figure S4: Lattice parameters of $CsMnCo(CN)_6$ from the same part of the sample such that the X-ray dose increases linearly with measurement number.

3 Variable-pressure data

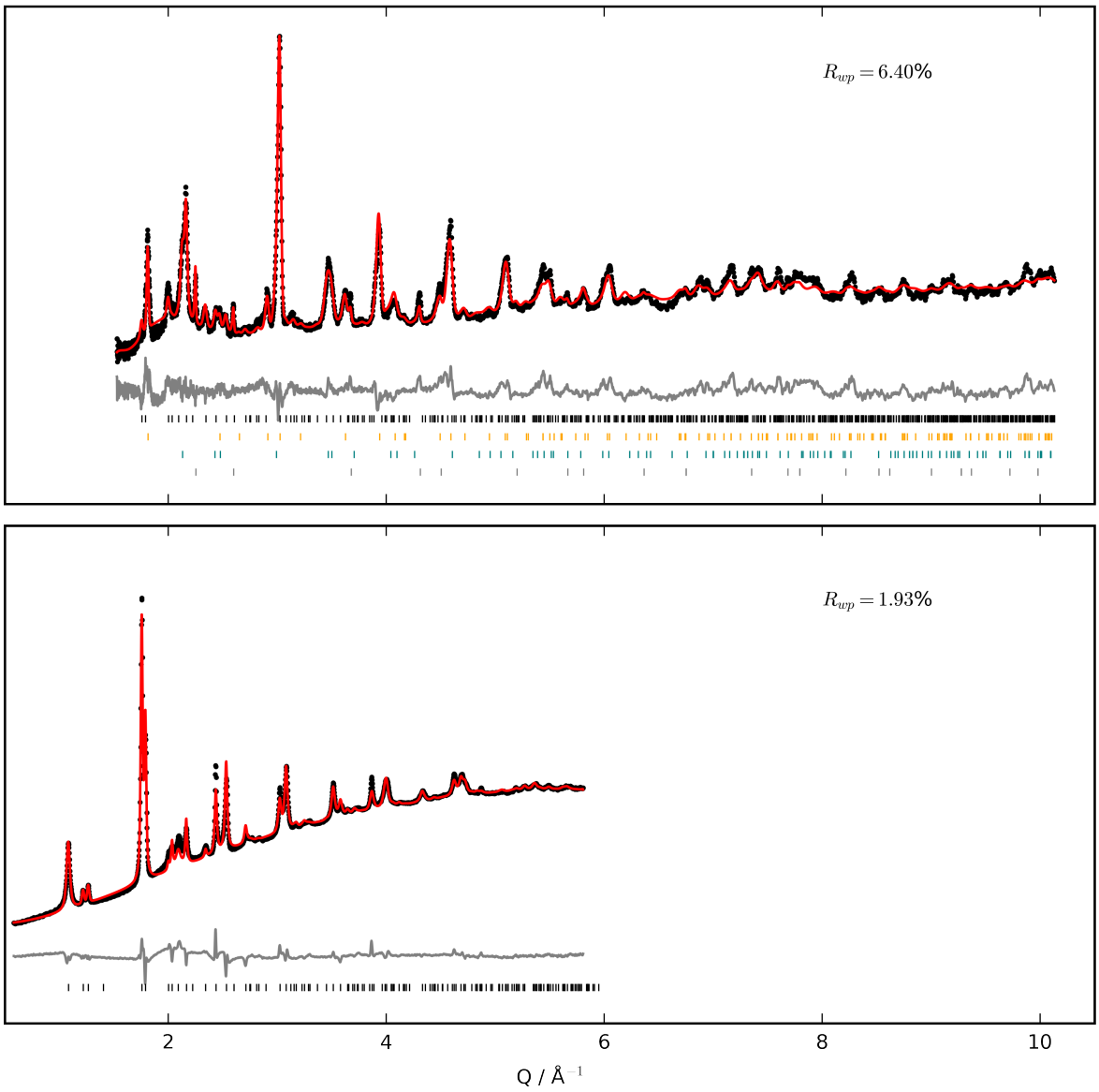

Figure S5: The Rietveld fit of the high-pressure phase of $CsMnCo(CN)_6$ in $P\bar{4}n2$ at 3.7 GPa. Experimental data are shown in black, the fit in red, the residuals in grey and allowed reflections indicated by vertical bars, where black corresponds to $CsMnCo(CN)_6$, yellow to Al_2O_3, teal to ZrO_2, and grey to Pb. The top panel shows the neutron data and the lower panel the X-ray data. The individual R_{wp} values for the two refinements are given; overall $R_{wp} = 4.16\%$.

Table S3: Crystallographic details determined by Rietveld refinement of combined X-ray and neutron diffraction data for $CsMnCo(CN)_6$ at 3.7 GPa. CSD: 2196070.

Space group	$P\bar{4}n2$
a / Å	7.0193(5)
c / Å	10.3129(12)
V / Å^3	508.12(10)
Z	2
R_{wp}	4.16%

Atom	occ	Wyckoff site	x	y	z	B_{iso}* / Å^2
Cs	0.811(5)	2c	0	0.5	0.25	2.24(18)
Cs	0.189(5)	2d	0	0.5	0.75	2.24
Mn	1	2a	0	0	0	2.24
Co	1	2b	0	0	0.5	2.24
N	1	8i	0.742(3)	0.865(3)	0	2.24
N	1	4e	0	0	0.196(2)	2.24
C	1	8i	0.668(4)	0.720(4)	0	2.24
C	1	4e	0	0	0.306(3)	2.24

* B_{iso} constrained to be equal for all atoms.

Table S4: Variable-pressure lattice parameters of $CsMnCo(CN)_6$. Uncertainty is ± 0.1 GPa at all pressures.

p / GPa	a / Å	c / Å
2.27	7.2097(4)	10.3477(8)
2.49	7.1725(4)	10.3468(7)
2.66	7.1450(5)	10.3456(8)
2.76	7.1323(4)	10.3437(7)
2.95	7.1025(4)	10.3373(8)
3.05	7.0911(4)	10.3350(9)
3.10	7.0842(4)	10.3331(8)
3.17	7.0766(4)	10.3309(8)
3.24	7.0685(4)	10.3288(9)

Table S4: Variable-pressure lattice parameters of $CsMnCo(CN)_6$. Uncertainty is ± 0.1 GPa at all pressures.

p / GPa	a / Å	c / Å
3.32	7.0604(4)	10.3262(8)
3.39	7.0515(4)	10.3238(8)
3.46	7.0439(4)	10.3213(8)
3.55	7.0337(4)	10.3186(8)
3.63	7.0247(4)	10.3152(8)
3.71	7.0171(4)	10.3125(8)
3.82	7.0062(4)	10.3081(9)
3.87	7.0016(4)	10.3057(9)
3.95	6.9951(5)	10.3028(9)
4.03	6.9880(5)	10.2999(9)
4.10	6.9818(5)	10.2969(9)
4.19	6.9745(5)	10.2929(9)
4.27	6.9662(5)	10.2886(9)
4.35	6.9587(5)	10.2853(9)
4.44	6.9525(5)	10.2813(9)
4.52	6.9456(5)	10.2782(9)
4.65	6.9352(5)	10.2719(10)
4.74	6.9266(5)	10.2672(10)
4.98	6.9114(5)	10.2578(10)
5.01	6.9092(5)	10.2559(10)
5.08	6.9049(5)	10.2527(10)
5.18	6.8980(5)	10.2477(10)
5.32	6.8870(5)	10.2405(10)
5.69	6.8628(6)	10.2236(11)
5.78	6.8572(7)	10.2188(13)
5.92	6.8494(6)	10.2121(12)
6.03	6.8421(6)	10.2055(12)
6.17	6.8348(6)	10.1981(12)
6.38	6.8226(6)	10.1879(12)
6.65	6.8097(6)	10.1742(12)

Table S4: Variable-pressure lattice parameters of $CsMnCo(CN)_6$. Uncertainty is ± 0.1 GPa at all pressures.

p / GPa	a / Å	c / Å
6.74	6.8051(6)	10.1681(12)
6.83	6.8015(6)	10.1639(12)
6.93	6.7975(6)	10.1572(12)
7.04	6.7933(6)	10.1493(12)
7.12	6.7905(6)	10.1439(12)
7.24	6.7862(6)	10.1368(13)
7.32	6.7833(6)	10.1317(12)
7.40	6.7798(6)	10.1267(12)
7.50	6.7757(6)	10.1209(13)
7.63	6.7718(6)	10.1149(13)
7.73	6.7690(6)	10.1104(13)

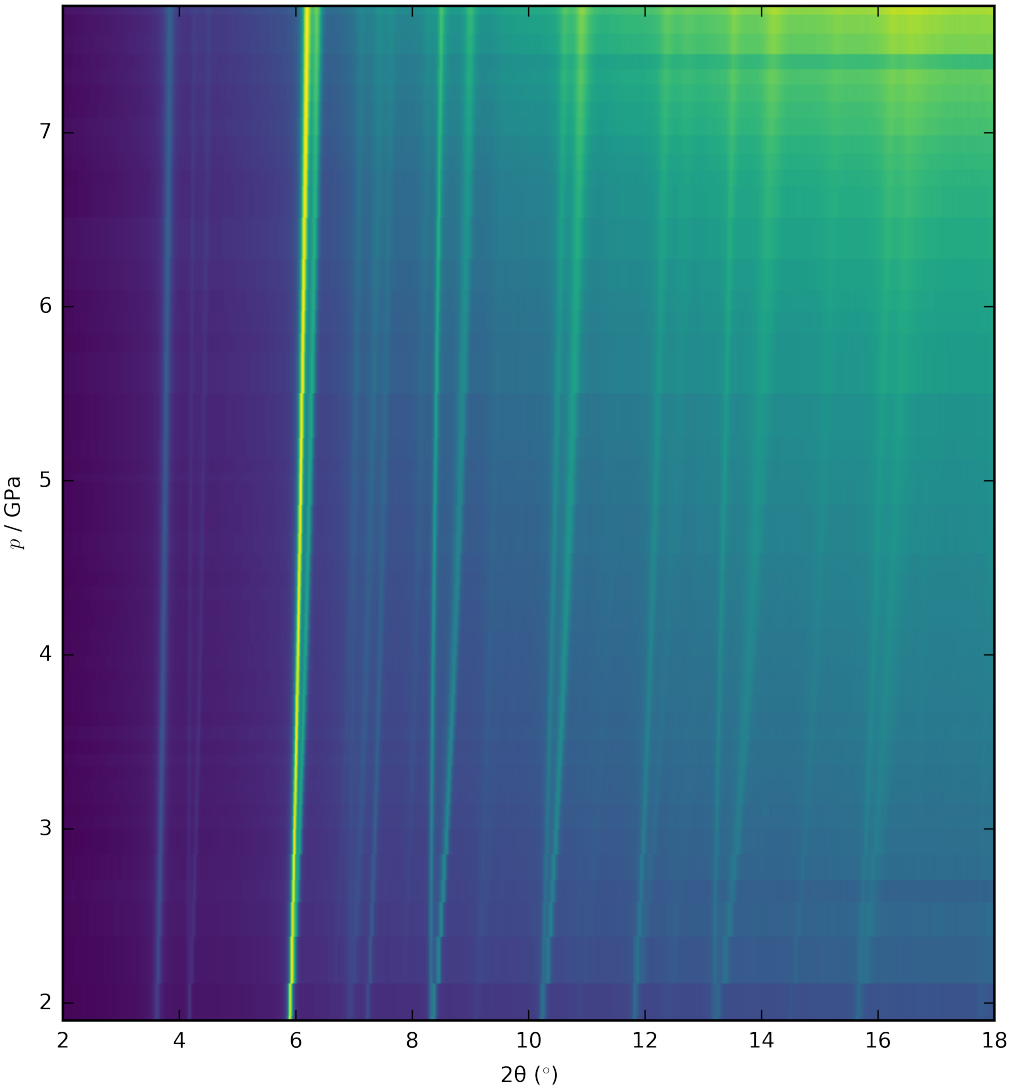

Figure S6: Variable-pressure X-ray diffraction patterns of $CsMnCo(CN)_6$. The intensities of the most intense reflection are normalised to unity. $\lambda = 0.3757\,\text{Å}$.

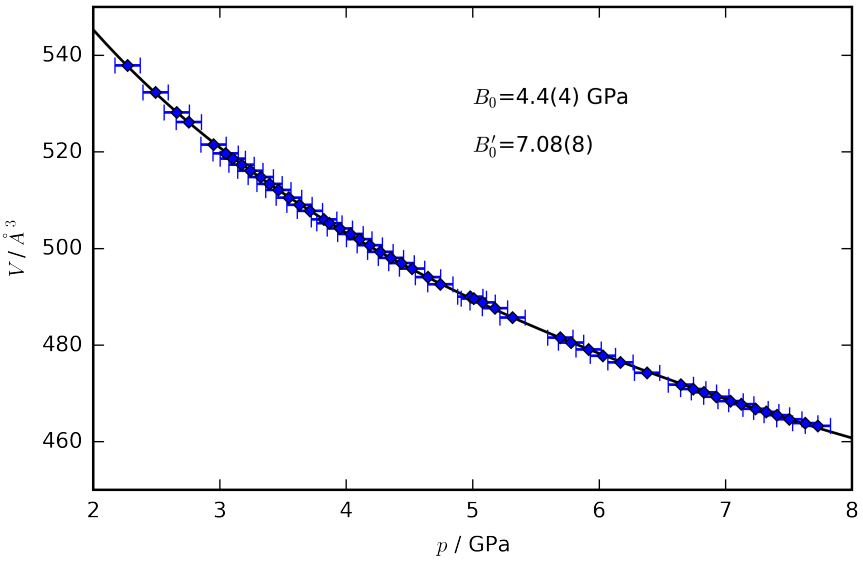

Figure S7: The cell volume of $CsMnCo(CN)_6$ as a function of pressure fitted with a third-order Murnaghan equation of state.

4 Variable-temperature data

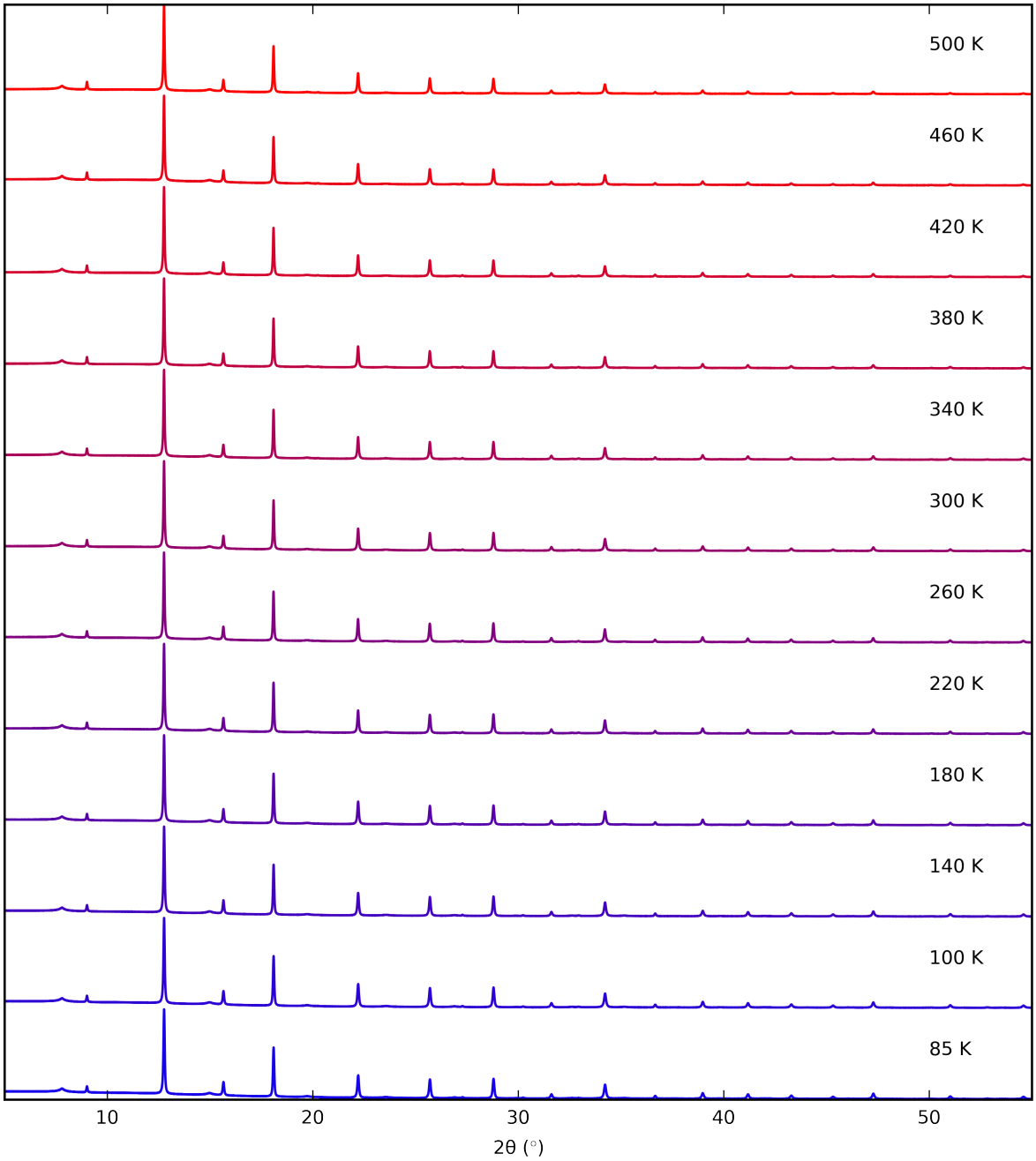

Figure S8: Variable-temperature X-ray diffraction patterns of $CsMnCo(CN)_6$. The intensities of the most intense reflection are normalised to unity. $\lambda = 0.82662\,\text{Å}$.

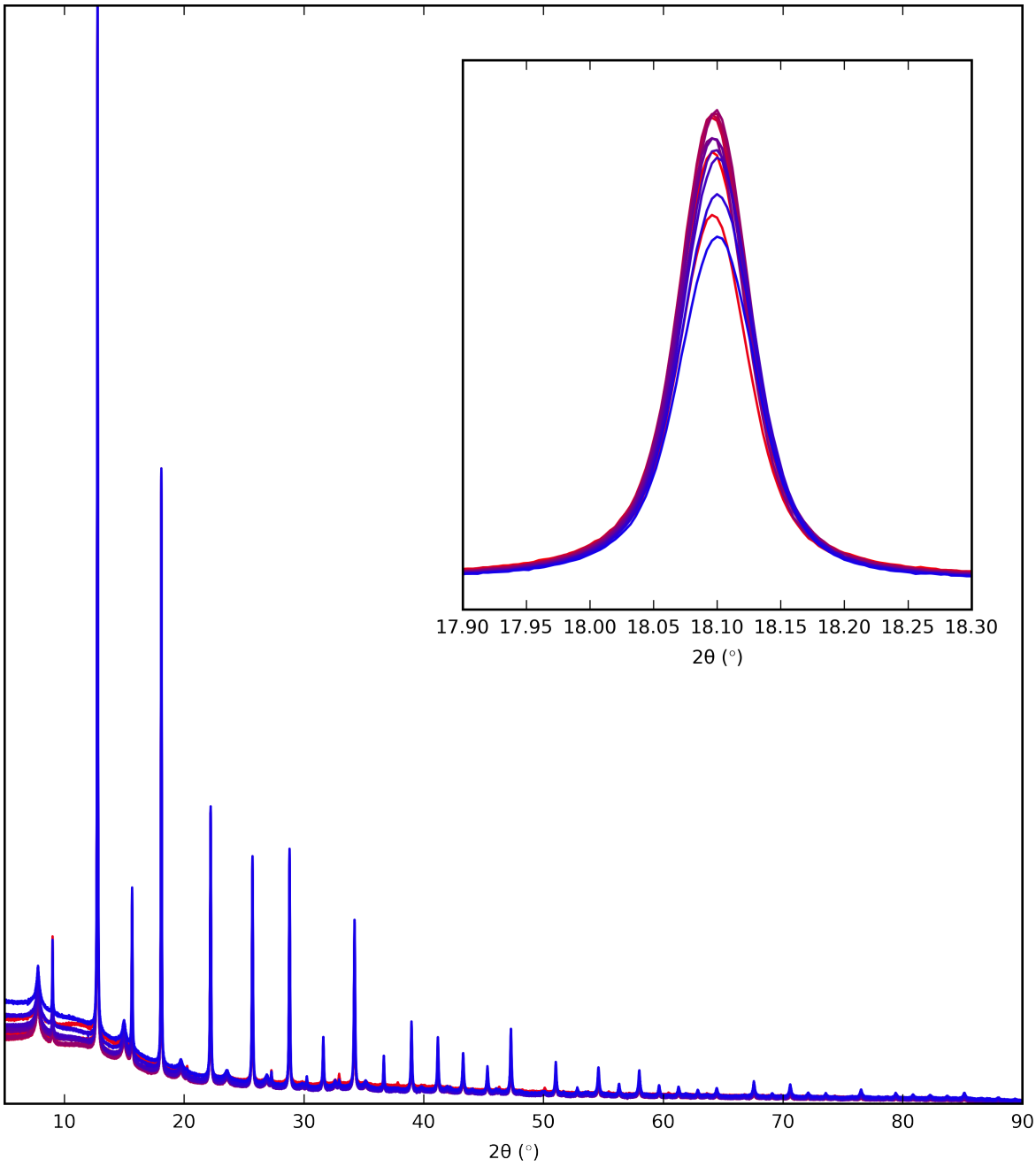

Figure S9: Variable-temperature X-ray diffraction patterns of $CsMnCo(CN)_6$, with the inset showing an enlarged view of the 400 reflection. The colour scheme is consistent with Fig. S8. $\lambda = 0.82662\,\text{Å}$.

Table S5: Variable-temperature lattice parameters of $CsMnCo(CN)_6$.

T / K	a / Å
500	10.50840(4)
460	10.50825(4)
420	10.50849(3)
380	10.50857(3)
340	10.50815(3)
300	10.50713(3)
260	10.50900(3)
220	10.50801(3)
180	10.50720(3)
140	10.50664(3)
100	10.50650(3)
85	10.50654(3)

5 Thermal expansion data

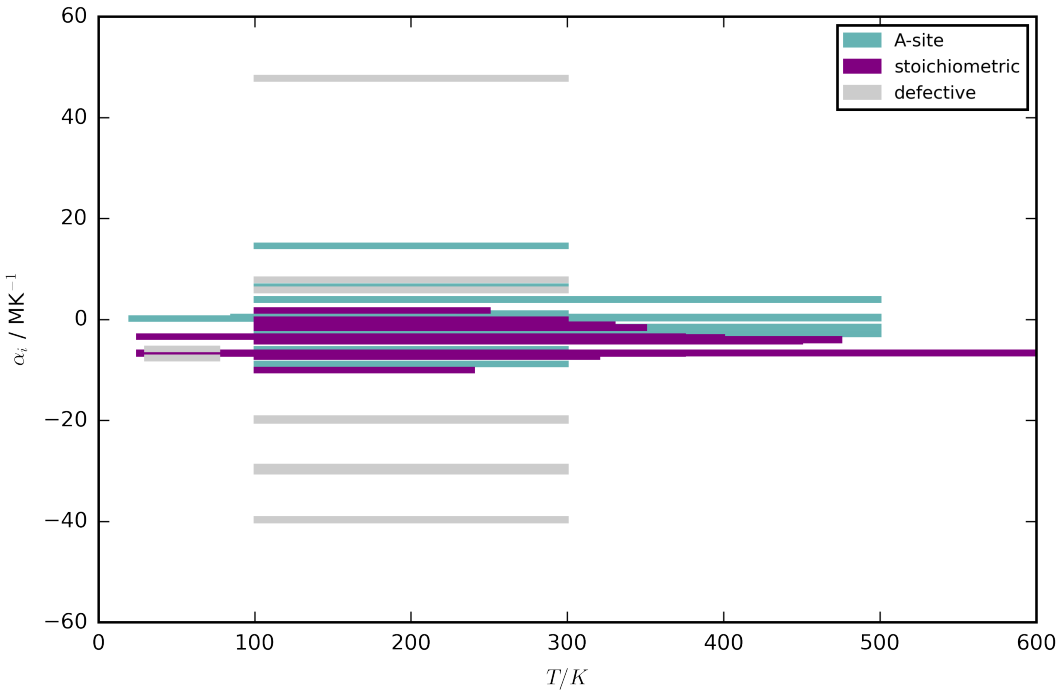

Figure S10: The linear coefficients of thermal expansion as a function of the studied temperature range for cubic PBAs.

Table S6: Collated thermal expansion coefficients of PBAs with formula $A_xM[M'(CN)_6]_y$, along with the relevant temperature range.

A	M	M′	x	y	α_a / MK^{-1}	$T_{\min}$	$T_{\max}$	Ref.
	Co	Co	0	0.33	−39.7(5.2)	100	300	11
	Zn	Fe	0	0.33	−39.6(6.2)	100	300	11
	Ni	Co	0	0.33	−30(4.4)	100	300	11
	Zn	Co	0	0.33	−29.7(2.8)	100	300	11
	Mn	Co	0	0.33	−29.2(5.8)	100	300	11
	Cu	Co	0	0.33	−20(1.2)	100	300	11
	Cu	Fe	0	0.33	−19.9(0.6)	100	300	11
	Fe	Co	0	0.33	−19.6(7)	100	300	11
	Cd	Pt	0	0.00	−10.02(11)	100	240	12
Cs	Cd	Fe	1	0.00	−8.8	100	300	13

Table S6: Collated thermal expansion coefficients of PBAs with formula $A_xM[M'(CN)_6]_y$, along with the relevant temperature range.

A	M	M′	x	y	α_a / MK^{-1}	T_{min}	T_{max}	Ref.
	Mn	Co	0	0.33	−7.6	30	77	14
	Cd	Pt	0	0.00	−7.31(5)	100	320	15
	Cd	Pt	0	0.00	−6.69(5)	25	375	15
	Sc	Co	0	0.00	−6.6	25	600	16
	Mn	Pt	0	0.00	−6.58(9)	100	300	12
Rb	Zn	Fe	0.64	0.12	−5.9	100	300	13
	Mn	Co	0	0.33	−5.8	30	77	14
	Fe	Fe	0	0.00	−4.26	100	450	17
Cs	Zn	Fe	0.91	0.03	−4.1	100	300	13
	Ti	Co	0	0.00	−4.05	100	475	18
	Fe	Pt	0	0.00	−4.00(7)	100	315	12
	Ga	Fe	0	0.00	−3.95(5)	100	475	19
	Zn	Pt	0	0.00	−3.53(5)	100	400	12
	Zn	Pt	0	0.00	−3.38(9)	25	375	15
Na	Ga	Fe	0.25	0.00	−2.83(3)	100	500	20
Rb	Fe	Fe	0.78	0.17	−2.1	100	300	13
	Co	Pt	0	0.00	−1.60(6)	100	350	12
Na	Ga	Fe	0.5	0.00	−1.51(2)	100	500	20
	Fe	Co	0	0.07	−1.47(1)	4.2	300	21
	Ni	Pt	0	0.00	−1.02(11)	100	330	12
Cs	Ni	Fe	0.7	0.10	−0.4	100	300	13
	Ti	Co	0	0.00	−0.023	100	300	18
Cs	Fe	Fe	0.98	0.10	0	100	300	13
Rb	Ni	Fe	0.46	0.18	0.1	100	300	13
Cs	Mn	Fe	0.94	0.09	0.2	20	200	22
Na	Ga	Fe	1	0.00	0.30(2)	100	500	20
Cs	Mn	Co	1	0.00	0.46(7)	85	500	this work
Rb	Mn	Fe	0.97	0.01	1.17(5)	230	300	23
	Zn	Pt	0	0.00	1.82(15)	100	250	15
Na	Ga	Fe	1	0.00	3.98(4)	100	500	20

Table S6: Collated thermal expansion coefficients of PBAs with formula $A_xM[M'(CN)_6]_y$, along with the relevant temperature range.

A	M	M′	x	y	α_a / MK^{-1}	T_{min}	T_{max}	Ref.
	Ni	Fe	0	0.33	5.9(1.9)	100	300	11
Cs	Co	Fe	0.91	0.16	6.5	100	300	13
	Co	Fe	0	0.33	7.9(5.1)	100	300	11
Rb	Co	Fe	0.49	0.20	14.6	100	300	13
	Mn	Fe	0	0.33	47.8(3.4)	100	300	11

6 References

(S1) C. Prescher and V. B. Prakapenka, *High Pressure Res.*, 2015, **35**, 223–230.

(S2) C. L. Bull, N. P. Funnell, M. G. Tucker, S. Hull, D. J. Francis and W. G. Marshall, *High Pressure Res.*, 2016, **36**, 493–511.

(S3) O. Arnold, J. C. Bilheux, J. M. Borreguero, A. Buts, S. I. Campbell, L. Chapon, M. Doucet, N. Draper, R. Ferraz Leal, M. A. Gigg, V. E. Lynch, A. Markvardsen, D. J. Mikkelson, R. L. Mikkelson, R. Miller, K. Palmen, P. Parker, G. Passos, T. G. Perring, P. F. Peterson, S. Ren, M. A. Reuter, A. T. Savici, J. W. Taylor, R. J. Taylor, R. Tolchenov, W. Zhou and J. Zikovsky, *Nucl. Instrum. Methods Phys. Res., Sect. A*, 2014, **764**, 156–166.

(S4) G. S. Pawley, *J. Appl. Cryst.*, 1981, **14**, 357–361.

(S5) H. M. Rietveld, *Acta Crystallogr.*, 1967, **22**, 151–152.

(S6) A. A. Coelho, *J. Appl. Cryst.*, 2018, **51**, 210–218.

(S7) B. J. Campbell, H. T. Stokes, D. E. Tanner and D. M. Hatch, *J. Appl. Cryst.*, 2006, **39**, 607–614.

(S8) M. J. Cliffe and A. L. Goodwin, *J. Appl. Cryst.*, 2012, **45**, 1321–1329.

(S9) F. D. Murnaghan, *Proc. Natl. Acad. Sci. U.S.A*, 1944, **30**, 244–247.

(S10) R. J. Angel, J. Gonzalez-Platas and M. Alvaro, *Z. Kristallogr.*, 2014, **229**, 405–419.

(S11) S. Adak, L. L. Daemen, M. Hartl, D. Williams, J. Summerhill and H. Nakotte, *J. Solid State Chem.*, 2011, **184**, 2854–2861.

(S12) K. W. Chapman, P. J. Chupas and C. J. Kepert, *J. Am. Chem. Soc.*, 2006, **128**, 7009–7014.

(S13) T. Matsuda, J. E. Kim, K. Ohoyama and Y. Moritomo, *Phys. Rev. B*, 2009, **79**, 172302.

(S14) K. W. Chapman, P. J. Chupas, E. R. Maxey and J. W. Richardson, *Chem. Commun.*, 2006,

4013–4015.

(S15) A. L. Goodwin, K. W. Chapman and C. J. Kepert, *J. Am. Chem. Soc.*, 2005, **127**, 17980–17981.

(S16) Q. Gao, Y. Sun, N. Shi, R. Milazzo, S. Pollastri, L. Olivi, Q. Huang, H. Liu, A. Sanson, Q. Sun, E. Liang, X. Xing and J. Chen, *Scr. Mater.*, 2020, **187**, 119–124.

(S17) N. Shi, Q. Gao, A. Sanson, Q. Li, L. Fan, Y. Ren, L. Olivi, J. Chen and X. Xing, *Dalton Trans.*, 2019, **48**, 3658–3663.

(S18) Q. Gao, X. Shi, A. Venier, A. Carnera, Q. Huang, H. Wu, J. Chen, A. Sanson and E. Liang, *Inorg. Chem.*, 2020, **59**, 14852–14855.

(S19) Q. Gao, N. Shi, Q. Sun, A. Sanson, R. Milazzo, A. Carnera, H. Zhu, S. H. Lapidus, Y. Ren, Q. Huang, J. Chen and X. Xing, *Inorg. Chem.*, 2018, **57**, 10918–10924.

(S20) Q. Gao, N. Shi, A. Sanson, Y. Sun, R. Milazzo, L. Olivi, H. Zhu, S. H. Lapidus, L. Zheng, J. Chen and X. Xing, *Inorg. Chem.*, 2018, **57**, 14027–14030.

(S21) S. Margadonna, K. Prassides and A. N. Fitch, *J. Am. Chem. Soc.*, 2004, **126**, 15390–15391.

(S22) T. Matsuda, H. Tokoro, H. Hashimoto and S.-i. Ohkoshi, *Dalton Trans.*, 2006, 5046–5050.

(S23) H. Tokoro, K. Nakagawa, K. Imoto, F. Hakoe and S.-i. Ohkoshi, *Chem. Mater.*, 2012, **24**, 1324–1330.